Octacoordinate Metal Carbonyls of Lanthanum and Cerium: Experimental Observation and Theoretical Calculation

ARTICLE *in* THE JOURNAL OF PHYSICAL CHEMISTRY A · SEPTEMBER 2014

Impact Factor: 2.69 · DOI: 10.1021/jp504079k · Source: PubMed

6 AUTHORS, INCLUDING:

Hua Xie
Chinese Academy of Sciences
27 PUBLICATIONS **110** CITATIONS
SEE PROFILE

Zhengbo Qin
Anhui Normal University
27 PUBLICATIONS **110** CITATIONS
SEE PROFILE

Zichao Tang
Chinese Academy of Sciences
67 PUBLICATIONS **517** CITATIONS
SEE PROFILE

Xiaopeng Xing
Tongji University
36 PUBLICATIONS **494** CITATIONS
SEE PROFILE

THE JOURNAL OF PHYSICAL CHEMISTRY A

Article

pubs.acs.org/JPCA

Octacoordinate Metal Carbonyls of Lanthanum and Cerium: Experimental Observation and Theoretical Calculation

Hua Xie,[†] Jie Wang,[‡,§] Zhengbo Qin,[†] Lei Shi,[†] Zichao Tang,*[,†] and Xiaopeng Xing*[,‡]

[†]State Key Laboratory of Molecular Reaction Dynamics, Dalian Institute of Chemical Physics, Chinese Academy of Sciences, Dalian 116023, China

[‡]Department of Chemistry, Tongji University, 1239 Siping Road, Shanghai 200092, China

Supporting Information

ABSTRACT: The octacoordinate metal carbonyls $La(CO)_8^+$ and $Ce(CO)_8^+$ were observed in laser vaporization of La and Ce in pure CO gas. The peak intensities in the mass spectra, the infrared photodissociation spectra, and the theoretical calculations indicate that all CO ligands in these two complexes are bonded with the central metal atoms. The CO stretching frequencies in $La(CO)_8^+$ and $Ce(CO)_8^+$ are determined to be 2110 and 2108 cm^{-1}, respectively. Theoretical studies indicate that the most stable structures for $La(CO)_8^+$ and $Ce(CO)_8^+$ are an O_h geometry at its triplet state and a slightly distorted O_h geometry at its quartet state, respectively. These two complexes represent new octacoordinate metal carbonyls after previously determined $U(CO)_8^+$ and $Y(CO)_8^+$.

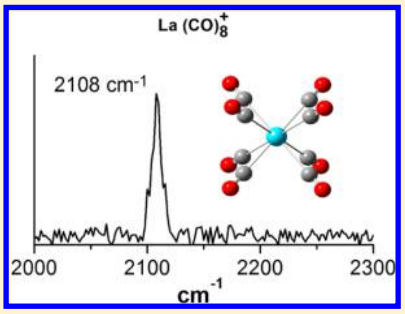

1. INTRODUCTION

Metal carbonyls have many applications, such as catalysts in industrial fields, precursors for complicated compounds, and antiknock agents in gasoline.[1] They are also of great importance in coordination chemistry, acting as prototypical models for some fundamental concepts.[2,3] Metal carbonyls synthesized in the condensed phase can be either neutral complexes or ionic units coexisting with suitable counterions. The metal atoms in these complexes are usually coordinatively saturated. With the development of matrix-isolation and gas-phase techniques, unsaturated metal carbonyls have been intensively studied, which are meaningful in elucidating the basic bonding principles between metal atoms and CO ligands.[4,5] At the same time, density function theory (DFT) calculations combined with these experiments were shown to be effective in predicting the structures of obtained complexes and interpreting the experimental observations.

In previous studies, an important topic for each metal carbonyl family was about the saturated coordination number of CO ligands. For transition metals, the saturation numbers can usually be rationalized using the 18-electron rule, which proposes that the electrons from 3σ orbitals of CO ligands and the valence electrons of the central atom form a $d^{10}s^2p^6$ noble gas configuration. The typical examples include the neutral complexes of $Ni(CO)_4$, $Fe(CO)_5$, and $Cr(CO)_6$,[2] and the ionic units isolated in matrix or gas phase, such as $Cu(CO)_4^+$, $Co(CO)_5^+$, and $Mn(CO)_6^+$.[4,5] This empirical rule has also been applied on some polynuclear metal carbonyls.[6,7] The early transition metals are expected to bond with more CO ligands, because they have fewer d electrons. The heptacoordinate $Nb(CO)_7^+$ and $Ta(CO)_7^+$ have been generated and characterized in gas phase.[8] The first discovered octacoordinated metal carbonyls is $U(CO)_8^+$,[9] in which uranium belongs to the actinide group. Very recently, our group predicted the enhanced stabilities of $Sc(CO)_8^+$ and $Y(CO)_8^+$, and this prediction was supported by the obtained mass spectra.[10] The octacoordinate $Y(CO)_8^+$ were recently confirmed by the infrared photodissociation study.[11]

In the periodic table, the lanthanide elements correspond to filling of the 4f electron shell. In most of their complexes, the lanthanide elements tend to be trivalent and bond with electronegative atoms, such as O, N, and Cl.[12] In the solid network structures containing lanthanide metals and a CO constituent, lanthanide atoms prefer to coordinate with the O atom.[13−15] The metal carbon coordination were usually identified in the unsaturated lanthanide carbonyls trapped in solid matrix.[16−21] In this work, we reported the observation of $La(CO)_8^+$ and $Ce(CO)_8^+$ generated in gas phase. The mass spectra, the theoretical calculations, and the infrared dissociation spectra indicate that eight CO ligands in each case chemically bond with the central metal atom through the metal carbon coordination.

2. EXPERIMENTAL METHOD

The experiments were carried out on a homemade apparatus, consisting of a laser vaporization ion source and a tandem time-of-flight (TOF) mass spectrometer. Figure 1 shows its schematic diagram. The ion source has been described in our previous studies.[10] Briefly, the 532 nm output of a Nd:YAG laser is focused to vaporize the rotating metal targets (their purities are higher than 99.9%) and various metal carbonyls are produced by reactions of vaporized species with pure CO

Received: April 26, 2014
Revised: September 9, 2014
Published: September 9, 2014

dx.doi.org/10.1021/jp504079k | J. Phys. Chem. A 2014, 118, 9380−9385

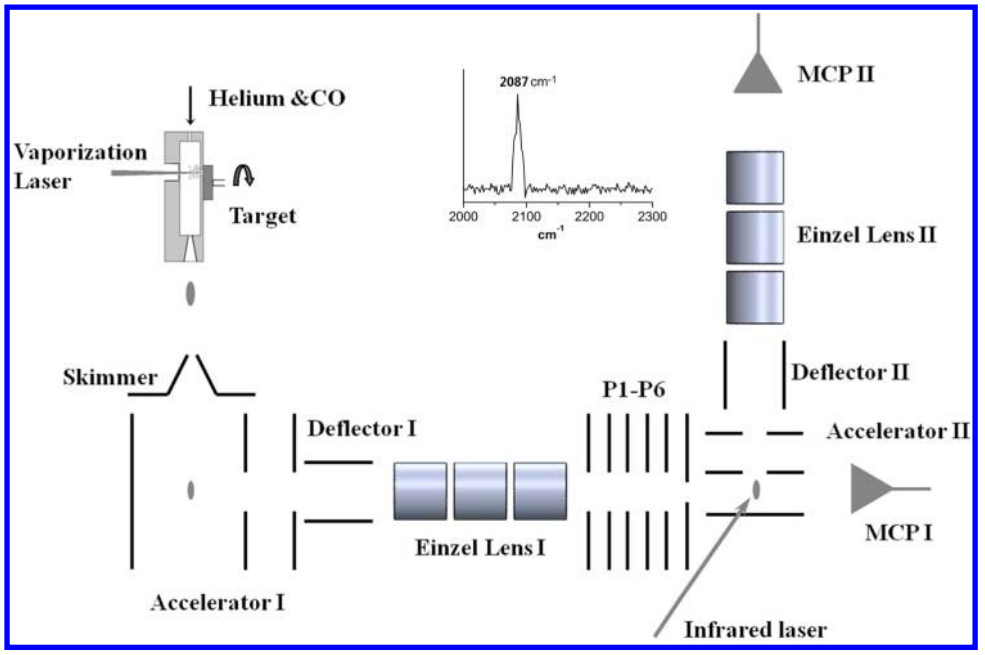

Figure 1. Schematic diagram of the experimental instrument consisting of a laser vaporization ion source and a tandem time-of-flight mass spectrometer. The inset shows the infrared photodissociation spectrum of $Y(CO)_8^+$.

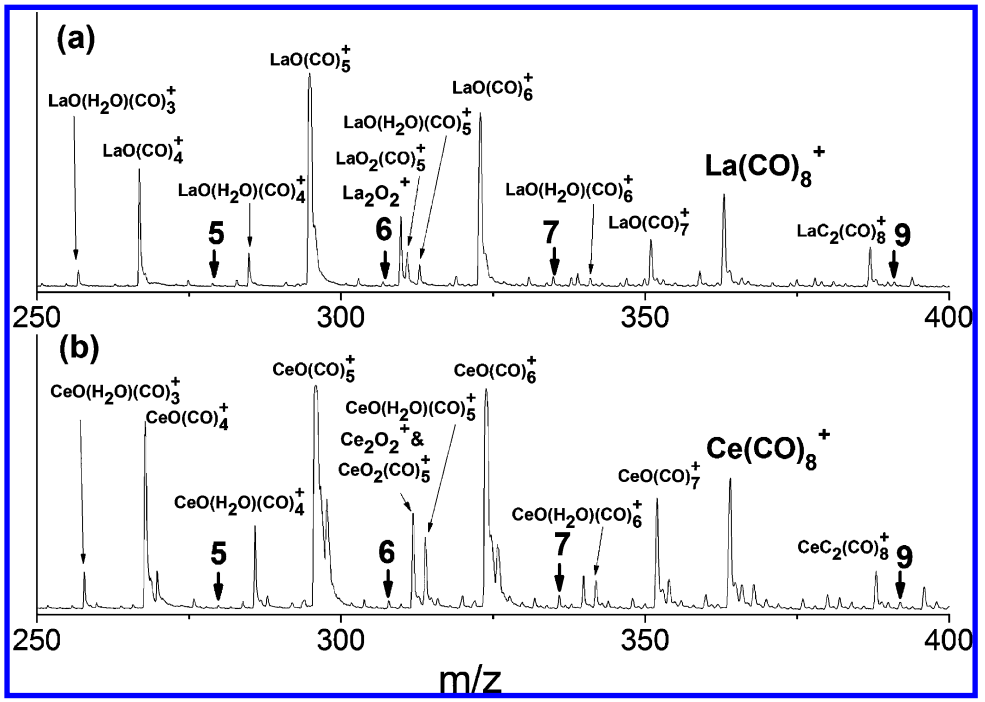

Figure 2. Mass spectra showing the cationic products from laser vaporization of (a) La and (b) Ce in pure CO gas. The bold numbers show the peaks of $M(CO)_n^+$, among which those of $La(CO)_8^+$ and $Ce(CO)_8^+$ are the strongest ones. The peaks of other products are also indicated.

(purity higher than 99.99%). The stagnation pressure of CO is about 8−10 atm and is introduced into a vacuum through a pulsed valve (General Valve, series 9). After free expansion, all products are skimmed into the acceleration region and the cationic species are analyzed using the first stage TOF. In the infrared (IR) photodissociation experiments, the cations of interest are mass selected and decelerated by a six plate stack (P1−P6 in Figure 1). The mass gate is composed of three plates P1−P3, among which P1 and P3 is grounded and P2 has a positive dc voltage. This dc voltage is 100 V higher than the acceleration voltage of the first stage TOF. When the cations of interest arrive at the mass gate, a negative 200 V pulse is superimposed on the dc voltage of P2 to let the selected ion past. In the deceleration region, P6 is always grounded and a adjustable negative voltage pulse is divided and applied on P4 and P5 after the selected cations past P4. These ions are decelerated in the electric field formed by P4, P5, and P6. The pulsed infrared laser is irradiated to the selected cationic packet in the acceleration region of the vertical second stage TOF, which analyzes the dissociation fragments and the left parent cations. The infrared spectra are obtained by recording the fragment cation yield as a function of the IR laser wavelength.

dx.doi.org/10.1021/jp504079k | J. Phys. Chem. A 2014, 118, 9380−9385

Typical spectra are obtained by scanning the infrared laser in step of 1 cm^{-1} and averaging about 300 laser shots at each wavelength.

The tunable infrared laser is generated by a KTP/KTA optical parametric oscillator/amplifier system (OPO/OPA, Laser Vision) pumped by a Continuum Surelite Nd:YAG laser. This system is tunable from 2000 to 5000 cm^{-1} with a line width of about 1 cm^{-1}. The infrared laser is loosely focused by a CaF_2 convex lens before entering the instrument vacuum. The wavelength of the OPO/OPA output has been calibrated by a commercial wavelength meter (Bristol, 821 Pulse Laser Wavelength Meter). We also took the infrared photodissociation spectra of $Y(CO)_8^+$ (the inset in Figure 1) and the obtained stretching frequency of its CO ligands is consistent with that recently reported by Duncan and coworkers.[11]

3. COMPUTATIONAL METHODS

DFT calculations were carried out to study the structures and bonding of $M(CO)_{7,8}^+$ (M = La and Ce). We initially optimized the structures in each state by using the B3LYP method[22] with LANL2DZ basis sets[23] for all elements. The optimizations of each species started from several geometries covering all reasonable chemical bonded structures. The obtained minimums were further optimized by using B3LYP and BP86 methods,[24] in which the 6-311+G (3df) basis sets were selected for C and O, and the SDD (SC-RECP, MWB28) basis set was selected for La and Ce.[25] In all these calculations, frequency analysis was applied to make sure the obtained structures were real minimums. The harmonic vibrational frequencies were calculated with analytic second derivatives based on the results from B3LYP/6-311+G (3df) & SDD level and BP86/6-311G +(3df) & SDD level, and then were scaled by the factors 0.967 and 1.008, respectively. These factors were determined by comparing the computed frequencies of free CO (2217 cm^{-1} at B3LYP level and 2126 cm^{-1} at BP86 level) and the experimental value (2143 cm^{-1}) of CO gas.

All calculations were performed using Gaussian 09 program.[26]

4. RESULTS AND DISCUSSION

4.1. Mass Spectra Indicating That $La(CO)_8^+$ and $Ce(CO)_8^+$ Are Coordinatively Saturated. In our ion source, pure CO reacts with the vaporized metal species very fast, preventing them from growing to larger clusters. Additionally, the extra energies in the vaporized plasma cause the dissociation of CO in the reaction channel, forming metal oxides and metal carbides. These species further absorb CO molecules and in some cases the water molecule in the background. The product series look different from the clean metal carbonyl series in vaporization of metals in helium with small percentage of CO.[27,28]

Parts a and b of Figure 2 display the cationic products when La and Ce are vaporized in CO, respectively. In spite of the complicated multistep reactions, a surprising one to one correspondence is found between the products shown in these two mass spectra. This could be an indication that the difference between the f atomic orbitals of La and Ce have little effects on their interactions with CO. The dominant product series in the two mass spectra were identified as $MO(CO)_n^+$ and $MO(H_2O)(CO)_n^+$ (M = La and Ce), in which the central metal atoms show their distinctive +3 valence. The peaks' intensities in these series change smoothly with the numbers of CO ligands. As for the expected $M(CO)_n^+$ (M = La and Ce) series, all members are very weak except $La(CO)_8^+$ and $Ce(CO)_8^+$. Both (a) and (b) of Figure 2 contains some other peaks such as $MO_2(CO)_5^+$ and $MC_2(CO)_8^+$ (M = La and Ce).

In our previous studies on scandium and yttrium carbonyls, we have estimated the pressures and temperatures in different regions of the ion source.[10] Then, the equilibrium intensities for the generated cationic metal carbonyls can roughly be estimated according to some known thermal dynamic parameters. For these lanthanum and cerium ones, the adsorption process and the van't Hoff equation are as follows:

$$M(CO)_{n-1}^+ + CO{=}M(CO)_n^+ \quad (1)$$

$$\ln K = \ln \frac{[M(CO)_n^+]}{[M(CO)_{n-1}^+] \times \frac{P_{co}}{p^\Theta}} = -\frac{\Delta_r H^\Theta}{RT} + \frac{\Delta_r S^\Theta}{R} \quad (2)$$

The $\Delta_r S^\Theta$ and $\Delta_r H^\Theta$ are around −100 J mol^{-1} K^{-1} and less than 10 kJ mol^{-1} for the physisorption of CO on the external shell of $(CO)_n^+$,[29] $H^+(CO)_n$,[30] and $CF_3^+(CO)_n$.[31] It is reasonable to assume that the $\Delta_r S^\Theta$ and $\Delta_r H^\Theta$ for the physisorption of CO on the external shell of $M(CO)_n^+$ (M = La and Ce) are at the same level. Then, the ratios $[M(CO)_n^+]/[M(CO)_{n-1}^+]$ in eq 2 were calculated to be less than 1/304 or 1/19 when P_{co} and T equal 10 atm and 300 K (estimated values in the reaction channel) or 0.4 atm and 120 K (estimated low limits after expansion cooling of the present source).[10] The peaks of $La(CO)_8^+$ and $Ce(CO)_8^+$ in Figure 2 are 1−2 orders of magnitude higher than their neighbors. Therefore, the eight CO ligands in each of these two complexes should be chemically bonded, making the central atom coordinatively saturated. The physisorption on the second shell likely starts from the ninth CO.

4.2. Theoretical Calculations for $La(CO)_{7,8}^+$ and $Ce(CO)_{7,8}^+$. We optimized the structures of $La(CO)_8^+$ and $Ce(CO)_8^+$ using DFT calculations. To estimate the bond energies of the last CO in these two complexes, we also studied the structures of $La(CO)_7^+$ and $Ce(CO)_7^+$. Figure 3 shows the

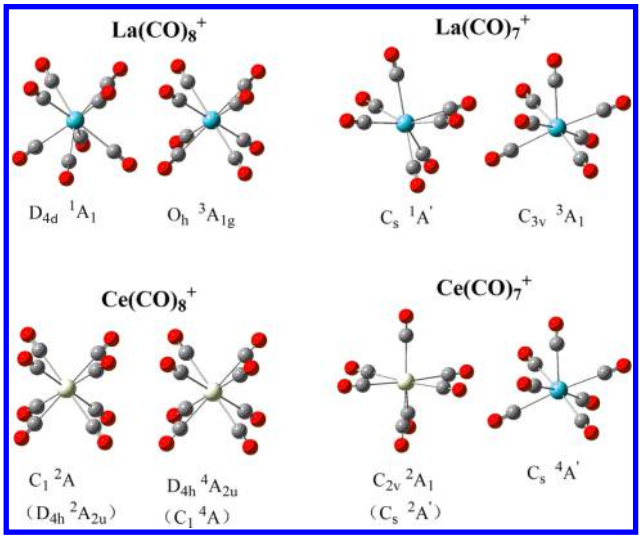

Figure 3. Theoretical structures of $M(CO)_{8,7}^+$ (M = La and Ce). Their geometries and electronic states are indicated. For some cases, the B3LYP method and the BP86 method give different results and those from the BP86 method are shown in the parentheses.

dx.doi.org/10.1021/jp504079k | J. Phys. Chem. A 2014, 118, 9380−9385

obtained geometrical structures and their electronic states. Table 1 displays the relative energies of the optimized structures and the computed bonding energies of the last CO in $La(CO)_8^+$ and $Ce(CO)_8^+$.

Table 1. Relative Energies of $M(CO)_{8,7}^+$ (M = La and Ce) and the Bond Energies of the Last CO in $M(CO)_8^+$ (M = La and Ce) from Theoretical Calculations

		relative energy[a]		$\Delta E[M(CO)_{n-1}^+ - CO]^a$	
complex	spin state	B3LYP	BP86	B3LYP	BP86
$La(CO)_8^+$	singlet	4.1	4.7	11.0	11.8
	triplet	0.0	0.0	10.7	12.1
$La(CO)_7^+$	singlet	4.5	4.4		
	triplet	0.0	0.0		
$Ce(CO)_8^+$	doublet	1.4	1.9	15.2	13.1
	quartet	0.0	0.0	10.5	11.9
$Ce(CO)_7^+$	doublet	6.2	3.2		
	quartet	0.0	0.0		

[a]All energies are in kcal/mol.

For $La(CO)_8^+$ and $La(CO)_7^+$, the B3LYP method and the BP86 method get consistent results. The predicted lowest structure for $La(CO)_8^+$ has an O_h geometry with the $^3A_{1g}$ state, in which eight CO ligands equally bonded on the central La atom. The singlet D_{4d} structure is more than 4 kcal/mol higher. For $La(CO)_7^+$, the C_{3v} geometry with the $^3A_1$ state is the lowest structure, which can be viewed as a capped octahedron. The similar C_{3v} structures have been predicted for $Sc(CO)_7^+$, $Y(CO)_7^+$, and $U(CO)_7^+$.[9,10] The singlet C_s structure of $La(CO)_7^+$ is more than 4 kcal/mol higher. The bond energies of the last CO in both triplet and singlet $La(CO)_8^+$ are more than 10 kcal/mol, which is among the strong chemical interaction range.

For $Ce(CO)_8^+$, both the B3LYP method and the BP86 method predict that the lowest structure has a quartet state and is slightly distorted from the O_h geometry. The B3LYP method predicts that the distortion is toward a D_{4h} geometry with the $^4A_{2u}$ state, whereas the BP86 method indicates that the final structure is distorted to a C_1 geometry with the ^4A state. For $Ce(CO)_7^+$, both the B3LYP and the BP86 methods predict that the lowest structure is a C_s geometry with the $^4A'$ state, which is slightly distorted from the C_{3v} structure predicted for $La(CO)_7^+$. The doublet structures for $Ce(CO)_8^+$ and $Ce(CO)_7^+$ were also shown in Figure 3 and Table 1. However, the calculations for these two structures always contain some spin contaminations. For example, the eigenvalue of the S^2 operator in the calculation of doublet $Ce(CO)_8^+$ is around 1.75 at either B3LYP or BP86 level, which is much higher than the expected 0.75 value for doublet species. The S^2 value of the predicted doublet $Ce(CO)_7^+$ is around 0.75 at B3LYP level, and 1.53 at BP86 level. These deviations indicate significant state mixing with higher spin states. Additionally, the theoretical energies for these doublet states are always higher in energy than the quartet ones at both B3LYP and BP86 levels. The bond energies of the last CO in both quartet and doublet $Ce(CO)_8^+$ are more than 10 kcal/mol, similar to the values predicted for $La(CO)_8^+$.

4.3. Comparisons between the Infrared Photodissociation Spectra and the Theoretical Calculations. We studied the infrared photodissociation of $La(CO)_8^+$ and $Ce(CO)_8^+$ around the stretching frequency region of CO. At the power intensity of ~10 mJ/cm^2, we only observed the dissociation channels corresponding to loss of one CO, and the dissociation ratio was always less than 10%. These observations are consistent with the calculated CO bonding energies of $La(CO)_8^+$ and $Ce(CO)_8^+$ shown in Table 1, which are apparently higher than the energies of the single photons here. The dissociations here should be multiphoton processes.

Parts a and c of Figure 4 display the obtained infrared photodissociation spectra of $La(CO)_8^+$ and $Ce(CO)_8^+$,

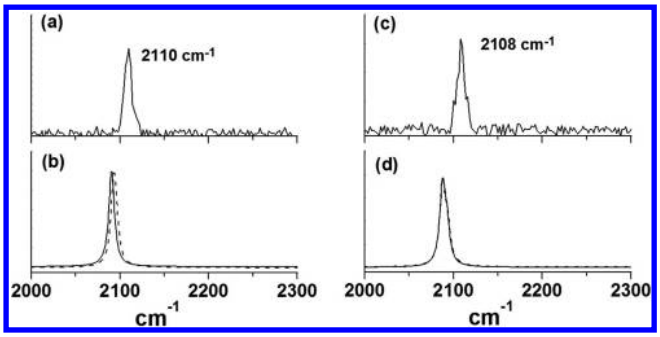

Figure 4. Experimental infrared photodissociation spectra of (a) $La(CO)_8^+$ and (c) $Ce(CO)_8^+$ and the simulated infrared spectra of (b) $La(CO)_8^+$ and (d) $Ce(CO)_8^+$. The simulation of the infrared spectra is based on the theoretical results from the B3LYP method. Each vibrational mode is represented by a Lorenz curve with the fwhm of 4 cm^{-1}. In (b) the black lines stand for the simulated spectra of the triplet or quartet state and the dashed lines stand for those of the singlet or doublet state. The black line and the dashed line in (d) completely overlap.

respectively. Each of them has only one clean band, which is at 2110 cm^{-1} for $La(CO)_8^+$ and 2108 cm^{-1} for $Ce(CO)_8^+$. These kinds of infrared spectra are likely signatures of the structures not far from a high symmetry. The theoretical frequencies for $La(CO)_{7,8}^+$ and $Ce(CO)_{7,8}^+$ at the B3LYP/6-311+G (3df) & SDD level are summarized in Table 2, and the simulated infrared spectra of $La(CO)_8^+$ and $Ce(CO)_8^+$ based on these values are shown in Figure 4b,d, respectively. The theoretical frequencies from calculations at BP86/6-311+G (3df) & SDD level are qualitatively consistent, which are summarized in Table S1 of the Supporting Information. The black line in Figure 4b,d in each simulated spectrum stands for

Table 2. Representative Frequencies of $La(CO)_{7,8}^+$ and $Ce(CO)_{7,8}^+$ from the B3LYP Method

complex	spin	representative frequencies from B3LYP theory[a]
$La(CO)_8^+$	singlet	2092 (312), 2092 (312), 2093 (1863), 2093 (1863), 2095 (2459)
	triplet	2090 (2420), 2090 (2420), 2090 (2420)
$La(CO)_7^+$	singlet	2080 (1255), 2081 (1358), 2087 (48), 2087 (1522), 2092 (733), 2092 (1563), 2153 (13)
	triplet	2062 (1046), 2077 (1571), 2077 (1565), 2097 (713), 2107 (894), 2107 (895), 2154 (22)
$Ce(CO)_8^+$	doublet	2088 (2365), 2088 (2364), 2093 (2160)
	quartet	2088 (2404), 2088 (2404), 2094 (2183)
$Ce(CO)_7^+$	doublet	2070 (1177), 2079 (2183), 2090 (2554), 2092 (46), 2095 (577)
	quartet	2059 (995), 2072 (1520), 2079 (1542), 2098 (814), 2104 (863), 2113 (777), 2155 (35)

[a]The frequencies are in wavenumbers and have been scaled by 0.967. The IR intensities in km/mol are shown in parentheses.

dx.doi.org/10.1021/jp504079k | J. Phys. Chem. A 2014, 118, 9380−9385

the triplet or the quartet state, and the dashed one stands for the singlet or the doublet one. We found that the structures with different spin states have very similar simulated spectra. Especially, those for the quartet and doublet states of $Ce(CO)_8^+$ completely overlap. All these simulated ones are in good agreement with the experiments shown in Figure 4a,c, even the comparison does not help to distinguish the different states for both $La(CO)_8^+$ and $Ce(CO)_8^+$. Comparing the experiment spectra with the predicted frequencies of $La(CO)_7^+$ and $Ce(CO)_7^+$ listed in Table 2 and Table S1 (Supporting Information), we can exclude the possible geometries of heptacoordinate $M(CO)_7^+$ (M = La or Ce) with a physisorbed CO.

4.4. Bonding in $La(CO)_8^+$ and $Ce(CO)_8^+$. The obtained CO stretching frequencies in $La(CO)_8^+$ and $Ce(CO)_8^+$ are red-shifted relative to that of free CO (2143 cm^{-1}) but are blue-shifted relative to those of previously reported $Y(CO)_8^+$ (2087 cm^{-1})[11] and $U(CO)_8^+$ (2080 cm^{-1}).[9] According to the Dewar–Chatt–Duncanson model, this red shift is attributed to the π back-bonding, in which electrons flow from the filled d-orbitals of the central metal to the π^* orbital of CO ligands.[2,4,5] In previous studies, the lowest structure of $Sc(CO)_8^+$ was predicted to be singlet and the structures of $Y(CO)_8^+$ with singlet and triplet states are nearly degenerate.[10,11] The enhanced stabilities of their singlet structures could be rationalized using the 18-electron rule, which proposes that the $d^{10}s^2p^6$ configuration is formed. In this work, the lowest structures of both $La(CO)_8^+$ and $Ce(CO)_8^+$ are predicted to be on the triplet state and the quartet state, respectively. Therefore, they cannot be rationalized using the 18-electron rules even their f atomic orbitals are not taken into account. We carried out bonding analysis on the theoretical structures of $La(CO)_8^+$ and compared the results with those of $Sc(CO)_8^+$ and $Y(CO)_8^+$. Figure 1S in Supporting Information shows the pictures and the energy levels (in eV) of the frontier orbitals in the theoretical structures of $M(CO)_8^+$ (M = Sc, Y and La) from B3LYP calculations. It seems that the frontier orbitals in the complexes with different central metal are quite similar, which include the π^* back-bonding HOMO and several lower-lying σ donation orbitals. The slight difference between $La(CO)_8^+$ and $Sc(CO)_8^+$ or $Y(CO)_8^+$ is that there are apparent f components from La in the frontier orbitals of $La(CO)_8^+$. This could be the physical origin making the triplet O_h structure more stable than the singlet D_{4d} one.

It is worth noting that the carbonyls of lanthanum and cerium are similar to previously reported uranium carbonyls in several aspects. For example, $U(CO)_8^+$ is also predicted to be on its second lowest spin state, a sextet, the CO stretching frequencies is red-shifted, the $U(CO)_7^+$ tend to be similar capped octahedral structures, and even more, the magic peak $UO_2(CO)_5^+$ in uranium carbonyls also appears in La and Ce mass spectra (as shown in Figure 2).[9] Therefore, we tend to believe that formation of octacoordinate metal carbonyls for La, Ce, and U could possibly originate from some common characters shared by these lanthanide and actinide metals.

5. CONCLUSIONS

The laser vaporization of La and Ce in pure CO gas generated $La(CO)_8^+$ and $Ce(CO)_8^+$, which were the highest peaks in the $La(CO)_n^+$ and $Ce(CO)_n^+$ series. Theoretical calculations predicted that $La(CO)_8^+$ is an O_h geometry with the $^3A_{1g}$ state, and $Ce(CO)_8^+$ is a slightly distorted O_h structure at its quartet state. The infrared photodissociation experiments showed that the CO stretching frequencies in $La(CO)_8^+$ and $Ce(CO)_8^+$ are 2110 and 2108 cm^{-1}, respectively. The π back-bonding contributes to this red shift. The metal carbonyls of La and Ce are similar to the previous reported uranium carbonyls in some aspects.

■ ASSOCIATED CONTENT

Supporting Information

The full ref 26, the representative frequencies of $La(CO)_{7,8}^+$ and $Ce(CO)_{7,8}^+$ at the BP86 level, and the frontier orbitals of the singlet and the triplet $M(CO)_8^+$ (M = Sc, Y and La). This material is available free of charge via the Internet at http://pubs.acs.org.

■ AUTHOR INFORMATION

Corresponding Authors

*Z. Tang. Tel.: +86-411-84379365. Fax: +86-411-84675584. Email: zctang@dicp.ac.cn.

*X. Xing. Tel.: +86-411-84379365. Fax: +86-411-84675584. Email: zctang@dicp.ac.cnxingxp@tongji.edu.cn.

Present Address

§Aluminum Corporation of China Limited, 62, Xizhimen North Street, Beijing, 100082, China.

Notes

The authors declare no competing financial interest.

■ ACKNOWLEDGMENTS

This work was supported by the National Natural Science Foundation of China (Grant No. 21073186, 21273233, 21103226, 21273278) AND the Ministry of Science and Technology of China (Grant No. 2011YQ09000505). The calculations were carried out on the Deepcomp7000 of Supercomputing Center, Computer Network Information Center of Chinese Academy of Sciences. We thank Prof. Ling Jiang for his support in the tunable infrared laser system.

■ REFERENCES

(1) Hartwig, J. F. *Organotransition Metal Chemistry: From Bonding to Catalysis*; University Science Books: Sausalito, CA, 2010.

(2) Cotton, F. A.; Wilkinson, G.; Murillo, C. A.; Bochmann, M. *Advanced Inorganic Chemistry*, 6th ed.; Wiley: New York, 1999.

(3) Frenking, G.; Frohlich, N. The Nature of the Bonding in Transition-Metal Compounds. *Chem. Rev.* **2000**, *100*, 717–774.

(4) Zhou, M. F.; Andrews, L.; Bauschlicher, C. W. Spectroscopic and Theoretical Investigations of Vibrational Frequencies in Binary Unsaturated Transition-Metal Carbonyl Cations, Neutrals, and Anions. *Chem. Rev.* **2001**, *101*, 1931–1961.

(5) Ricks, A. M.; Reed, Z. E.; Duncan, M. A. Infrared Spectroscopy of Mass-Selected Metal Carbonyl Cations. *J. Mol. Spectrosc.* **2011**, *266*, 63–74.

(6) Wang, G.; Cui, J.; Chi, C.; Zhou, X.; Li, Z. H.; Xing, X.; Zhou, M. Bonding in Homoleptic Iron Carbonyl Cluster Cations: A Combined Infrared Photodissociation Spectroscopic and Theoretical Study. *Chem. Sci.* **2012**, *3*, 3272–3279.

(7) Cui, J.; Xing, X.; Chi, C.; Wang, G.; Liu, Z.; Zhou, M. Infrared Photodissociation Spectra of Mass-Selected Homoleptic Dinuclear Palladium Carbonyl Cluster Cations in the Gas Phase. *Chin. J. Chem.* **2012**, *30*, 2131–2137.

(8) Ricks, A. M.; Reed, Z. D.; Duncan, M. A. Seven-Coordinate Homoleptic Metal Carbonyls in the Gas Phase. *J. Am. Chem. Soc.* **2009**, *131*, 9176–9177.

(9) Ricks, A. M.; Gagliardi, L.; Duncan, M. A. Infrared Spectroscopy of Extreme Coordination: The Carbonyls of U^+ and UO_2^+. *J. Am. Chem. Soc.* **2010**, *132*, 15905–15907.

(10) Xing, X. P.; Wang, J.; Xie, H.; Liu, Z. L.; Qin, Z. B.; Zhao, L. J.; Tang, Z. C. Octacoordinate Metal Carbonyls of Scandium and Yttrium: Theoretical Calculations and Experimental Observation. *Rapid Commun. Mass Spectrom.* **2013**, *27*, 1403−1409.
(11) Brathwaite, A. D.; Maner, J. A.; Duncan, M. A. Testing the Limits of the 18-Electron Rule: The Gas-Phase Carbonyls of Sc^+ and Y^+. *Inorg. Chem.* **2014**, *53*, 1166−1169.
(12) Mishra, S. Anhydrous Scandium, Yttrium, Lanthanide and Actinide Halide Complexes with Neutral Oxygen and Nitrogen Donor Ligands. *Coord. Chem. Rev.* **2008**, *252*, 1996−2025.
(13) Ye, J.; Su, H.; Bai, F.; Du, Y.; Zhang, Y. Synthesis, Crystal Structure and Properties of a New Lanthanide-Transition Metal Carbonyl Cluster. *Appl. Organomet. Chem.* **2009**, *23*, 86−90.
(14) Liu, S. M.; Plecnik, C. E.; Shore, S. G. Lanthanide-Transition Metal Carbonyl Complexes: Architectures Derived from Isocarbonyl Polymeric Arrays. *Compt. Rend. Chim.* **2005**, *8*, 1827−1837.
(15) Plecnik, C. E.; Liu, S. M.; Shore, S. G. Lanthanide-Transition-Metal Complexes: From Ion Pairs to Extended Arrays. *Acc. Chem. Res.* **2003**, *36*, 499−508.
(16) Klotzbucher, W. E.; Petrukhina, M. A.; Sergeev, G. B. Reactions of Samarium Atoms in Inert and Reactive Matrices. *Mendeleev Commun.* **1994**, 5−7.
(17) Xu, W. H.; Jin, X.; Chen, M. H.; Pyykko, P.; Zhou, M. F.; Li, J. Rare-Earth Monocarbonyls MCO: Comprehensive Infrared Observations and a Transparent Theoretical Interpretation for M = Sc; Y; La-Lu. *Chem. Sci.* **2012**, *3*, 1548−1554.
(18) Gong, Y.; Ding, C. F.; Zhou, M. F. Infrared Spectra of Oxygen-Rich Yttrium and Lanthanum Dioxygen/Ozonide Complexes in Solid Argon. *J. Phys. Chem. A* **2009**, *113*, 8569−8576.
(19) Zhou, M.; Jin, X.; Li, J. Reactions of Cerium Atoms and Dicerium Molecules with CO: Formation of Cerium Carbonyls and Photoconversion to CO-Activated Insertion Molecules. *J. Phys. Chem. A* **2006**, *110*, 10206−10211.
(20) Jiang, L.; Xu, Q. Reactions of Laser-Ablated La and Y Atoms with Co: Matrix Infrared Spectra and Dft Calculations of the $M(CO)_x$ and MCO^+ (M = La, Y; X=1−4) Molecules. *J. Phys. Chem. A* **2007**, *111*, 3271−3277.
(21) Xu, Q.; Jiang, L.; Zou, R. Q. Infrared-Spectroscopic and Density-Functional-Theory Investigations of the LaCO, $La_2[\eta^2(\mu_2$-C,O)], and C-$La_2(\mu$-C)(μ-O) Molecules in Solid Argon. *Chem.—Eur. J.* **2006**, *12*, 3226−3232.
(22) Becke, A. D. Density-Functional Thermochemistry. III. The Role of Exact Exchange. *J. Chem. Phys.* **1993**, *98*, 5648−5652.
(23) Hay, P. J.; Wadt, W. R. Ab Initio Effective Core Potentials for Molecular Calculations. Potentials for K to Au Including the Outermost Core Orbitals. *J. Chem. Phys.* **1985**, *82*, 299−310.
(24) Becke, A. D. Density-Functional Exchange-Energy Approximation with Correct Asymptotic-Behavior. *Phys. Rev. A* **1988**, *38*, 3098−3100.
(25) Dolg, M.; Stoll, H.; Preuss, H. Energy-Adjusted Ab Initio Pseudopotentials for the Rare Earth Elements. *J. Chem. Phys.* **1989**, *90*, 1730−1734.
(26) Frisch, M. J.; Trucks, G. W.; Schlegel, H. B.; Scuseria, G. E.; Robb, M. A.; Cheeseman, J. R.; Scalmani, G.; Barone, V.; Mennucci, B.; Petersson, G. A.; et al. *Gaussian 09*, Revision A02; Gaussian, Inc.: Wallingford, CT, 2009.
(27) Duncan, M. A. Invited Review Article: Laser Vaporization Cluster Sources. *Rev. Sci. Instrum.* **2012**, *83*, 041101−19.
(28) Wang, G.; Chi, C.; Cui, J.; Xing, X.; Zhou, M. Infrared Photodissociation Spectroscopy of Mononuclear Iron Carbonyl Anions. *J. Phys. Chem. A* **2012**, *116*, 2484−2489.
(29) Hiraoka, K.; Mori, T.; Yamabe, S. On the Formation of the Isomeric Cluster Ions $(CO)_n^+$. *J. Chem. Phys.* **1991**, *94*, 2697−2703.
(30) Hiraoka, K.; Mori, T. Gas-Phase Stabilities of Cluster Ions $H^+(CO)_2(CO)_n$,$H^+(N_2)_2(N_2)_n$, and $H^+(O_2)_2(O_2)_n$ with n = 1−14. *Chem. Phys.* **1989**, *137*, 345−352.
(31) Hiraoka, K.; Nasu, M.; Fujimaki, S.; Ignacio, E. W.; Yamabe, S. Gas-Phase Stability and Structure of the Cluster Ions $CF_3^+(CO)_n$, $CF_3^+(N_2)_n$, $CF_3^+(CF_4)_n$, and $CF_4H^+(CF_4)_n$. *J. Phys. Chem.* **1996**, *100*, 5245−5251.